Journal of Materials Chemistry A

Accepted Manuscript

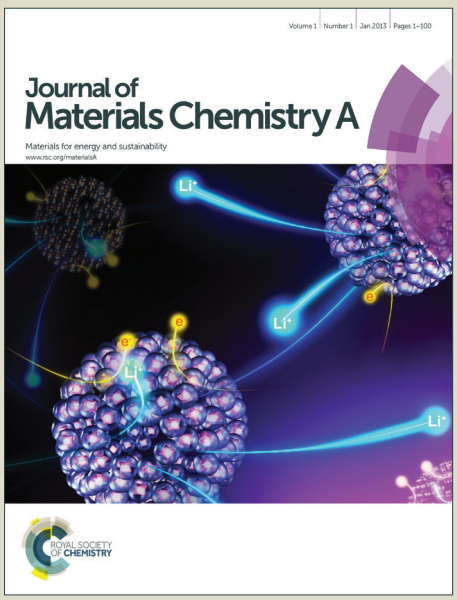

ROYAL SOCIETY OF CHEMISTRY

www.rsc.org/materialsA

Graphical abstract

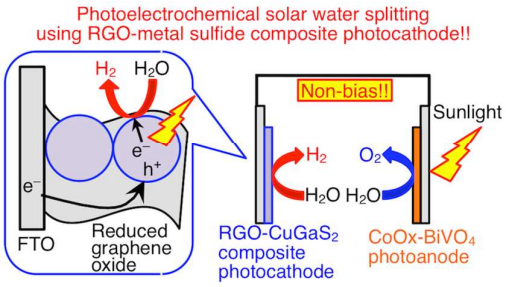

Textual abstract

The photoelectrochemical cell consisting of the enhanced RGO-$CuGaS_2$ composite photocathode and a CoOx-loaded $BiVO_4$ photoanode gave photocurrent under simulated sunlight irradiation without any external applied bias.

Journal Name

RSCPublishing

ARTICLE

Solar hydrogen evolution using $CuGaS_2$ photocathode improved by incorporating reduced graphene oxide

Cite this: DOI: 10.1039/x0xx00000x

A. Iwase*[a,b] Y. H. Ng[c] R. Amal[c] and A. Kudo*[a,b]

Received 00th January 2012,
Accepted 00th January 2012

DOI: 10.1039/x0xx00000x

www.rsc.org/

The effectiveness of reduced graphene oxide (RGO) in water reduction on a $CuGaS_2$ photocathode was demonstrated. Graphene oxide was photocatalytically reduced over $CuGaS_2$ particles under visible light irradiation to give an RGO-$CuGaS_2$ composite. The incorporated RGO dramatically enhanced the cathodic photocurrent of the $CuGaS_2$ photoelectrode under visible light irradiation. Detection of evolved H_2 indicated that the enhanced cathodic photocurrent was used for water reduction to H_2. Upon combining the developed RGO-$CuGaS_2$ composite photocathode with a $BiVO_4$ photoanode loaded with CoOx cocatalyst, photocurrent and the corresponding H_2 evolution were successfully observed without applying an external bias between both photoelectrodes under simulated sunlight irradiation.

Introduction

Photocatalytic and photoelectrochemical water splitting has been extensively studied as artificial photosynthesis.[1–4] An advantage of the photoelectrochemical water splitting is the separate H_2 evolution from O_2. Moreover, the band bending formed by an applied potential assists charge separation to give high performance in a photoelectrochemical reaction. In other words, a photocatalyst which thermodynamically possesses insufficient potential for water splitting can be used for photoelectrochemical water splitting.

The metal sulfides with narrow band gaps are a promising material group for photocatalytic hydrogen evolution under visible light irradiation.[2,5] However, the powdered metal sulfide photocatalyst requires sacrificial reagents to function steadily, because photogenerated holes in the sulfide particle oxidize the sulfide photocatalyst itself, resulting in photocorrosion. In other words, the metal sulfide particulate photocatalysts are not suitable for water splitting into H_2 and O_2. The disadvantage can be overcome by employing the metal sulfides in a photoelectrode system. Note that the metal sulfides have to be a p-type semiconductor if they are to be employed as a photocathode on which reduction reactions proceed. In this system, the photogenerated holes in the metal sulfide are removed from the electrode, resulting in suppressing photocorrosion and achieving the photoelectrochemical water splitting.[6,7] Therefore, the performance improvement of metal sulfide photoelectrode is a significant and attractive issue.

In a photoelectrode prepared by depositing the photocatalyst particles on a conductive substrate electrode, the interfaces of the particle-particle and the particle-substrate would be one of the recombination sites of photogenerated carries.[8] We have reported that the incorporation of a conductive reduced graphene oxide (RGO) improves the electrochemical performance of $BiVO_4$ with an n-type semiconductor character.[9] In this system, the RGO forms new and effective ways for the electron migration and boosts the electron migration from the photocatalyst particles to the conductive substrate electrode. Similar enhancement was observed for the n-type TiO_2 and WO_3 photoelectrodes.[10–12] These enhancements in the n-type semiconductor photoelectrode motivate us to investigate the effectiveness of RGO on the electrochemical performance of a p-type semiconductor photoelectrode. In order to achieve efficient water splitting using a photoelectrochemical cell consisting of a photocathode and a photoanode, development of a highly efficient photocathode is also significant.

In the present study, we focused on the established metal sulfide of $CuGaS_2$ with a p-type semiconductor character.[13–15] The RGO-$CuGaS_2$ composite was prepared by reducing GO over the $CuGaS_2$ under visible light irradiation, and the effectiveness of RGO in water splitting on a $CuGaS_2$ photoelectrode was investigated. Solar hydrogen production using a photoelectrochemical cell consisting of the developed RGO-$CuGaS_2$ composite photocathode and the Co-loaded $BiVO_4$ doped with Mo photoanode was also demonstrated.

Experimental

Synthesis of graphene oxide and $CuGaS_2$ powder.

Graphene oxide (GO) was synthesized from a commercially obtained graphite powder using Hummers's method.[16] The graphite was oxidized to graphene oxide by $KMnO_4$ in a sulfuric acid solution containing $NaNO_3$. The obtained GO was collected as dark brown powder by filtration.

$CuGaS_2$ was synthesized by a solid-state reaction. Starting materials of Cu_2S (Kojundo Chemical Lab, 99%) and Ga_2S_3 (Kojundo Chemical Lab, 99.99%) in a molar ratio of Cu:Ga=1:1.2 were mixed in an agate mortar. The mixed powder was encapsulated in a quartz tube after evacuation, and was subsequently calcined at 1073 K for 10h.

Preparation of RGO-$CuGaS_2$ composite

RGO-$CuGaS_2$ composite was prepared by photocatalytic reduction of GO over the $CuGaS_2$ under visible light irradiation. A certain amount of GO powder (5 wt% to $CuGaS_2$) and 0.3–0.5g of $CuGaS_2$ powder were dispersed in a 50 vol% of aqueous methanol solution (30 mL). The suspensions were stirred and bubbled with an Ar gas during visible light irradiation for 3 hours.

Characterization

The crystal phase of the obtained $CuGaS_2$ was assigned to chalcopyrite phase (Figure S1) by X-ray diffraction (Rigaku, MiniFlex). Diffuse reflectance spectra were obtained by a UV-vis-NIR spectrometer (JASCO, V-570) equipped with an integrator sphere and were converted to absorbance by the Kubelka-Munk method. The reduction state of GO was analyzed by X-ray photoelectron spectroscopy (Kratos Analytical, ESCA-3400). Morphology of the photocatalyst powder, composite, and photoelectrode was observed using a scanning electron microscope (JEOL, JSM-6700F). Electrochemical impedance spectra were obtained by AC impedance measurement using a frequency response analyzer (Solartron Analytical, Model 1260A). The measurement was carried out in 0.1 mol L^{-1} of an K_2SO_4 solution at 0.1 V of AC voltage over the frequency range from 0.01 Hz to 1 MHz.

Preparation of photoelectrode

$CuGaS_2$ and RGO-$CuGaS_2$ composite photoelectrodes were prepared by a drop-casting method. $CuGaS_2$ and RGO-$CuGaS_2$ composite powders were dispersed in ethanol (1 mg mL^{-1}) by sonication. The suspension was drop-casted on an FTO substrate (Asahi Glass) to obtain 1–2 mg cm^{-2} of $CuGaS_2$ on the FTO. The powder-loaded FTO was calcined at 773K for 2 hours in a N_2 atmosphere. The thickness of the deposited photocatalyst particles was determined using a 3D Laser Scanning Microscope (Keyence, VK-X200).

A $BiVO_4$ photoanode was prepared from an aqueous precursor solution according to the previous report.[17] A precursor-pasted FTO substrate was calcined at 673 K for 2 hours in air to obtain crystallized $BiVO_4$ on the FTO substrate. CoOx cocatalyst was loaded on the $BiVO_4$ photoelectrode by dropping a certain amount of an aqueous $Co(NO_3)$ solution and subsequent calcination at 673K for 2 hours in air.

Photoelectrochemical measurement

Photoelectrochemical properties were evaluated with three-electrode system consisting of working, Ag/AgCl reference, and Pt counter electrodes using a potentiostat (Hokuto Denko; HZ-5000 and HZ-7000). 0.1 mol L^{-1} of an aqueous K_2SO_4 solution was used as an electrolyte. A 300 W Xe lamp (Asahi Spectra, MAX-301) with a long-pass filter (Kenko, L42) was employed as a light source. H_2 and O_2 evolved were determined using gas chromatography (Shimadzu; MS-5A column, TCD, Ar carrier). The metal cations in the electrolyte after the photoelectrochemical measurement were analyzed by ICP-AES (Hitachi High-Tech Science, SPS3500) to see the durability of the photoelectrode. The detection limits of Cu and Ga are 1ppb and 10ppb, respectively.

A 300 W Xe lamp with band-pass filters was employed for measurement of incident photon to photocurrent efficiency (IPCE). The number of incident photons was measured using a photodiode head (OPHIRA; PD300-UV) and a power monitor (NOVA). IPCE was calculated as follows.

[IPCE%] = 1240x[Photocurrent density/μA cm^{-2}] / ([Wavelength/nm] x [Photon flux/W m^{-2}])

Photoelectrochemical water splitting was carried out using a two-electrode cell consisting of a RGO-$CuGaS_2$ composite photocathode and a Co-loaded $BiVO_4$ photoanode. A solar simulator (Asahi Spectra; HAL-320) was used as a light source. Solar energy conversion efficiency was calculated as follows.

[Solar energy conversion efficiency %] = 100 x [Photocurrent density/mA cm^{-2}] x (1.23–E_{apply}/V) / [Solar energy (AM1.5)/mW cm^{-2}]

Results and discussion

1. Characterization of RGO-$CuGaS_2$ composite

The suspension of the graphene oxide (GO) and $CuGaS_2$ powder was yellow as shown in Figure 1A. The color turned to darker upon irradiating visible light, implying that GO was reduced photocatalytically to reduced graphene oxide (RGO) by $CuGaS_2$, judging from the darker color of RGO (black) than that of GO (brown).[9,18,19] The oxidation state of GO was analyzed by XPS as shown in Figure 1B. The GO has typical three peaks due to carbon species with different surroundings of C–C, C–O, and C=O as previously reported.[20,21] The intensity of the peak of C–O dramatically decreased upon visible light irradiation, indicating that the GO was reduced to RGO. The similar decrease was observed, when TiO_2 and $BiVO_4$

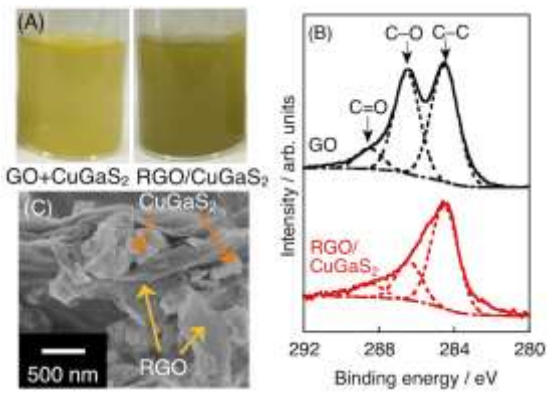

Figure 1 (A) Photographs of suspension of graphene oxide and $CuGaS_2$ before (left) and after (right) visible light irradiation, (B) C1s XPS spectra, and (C) SEM image of RGO-$CuGaS_2$ composite.

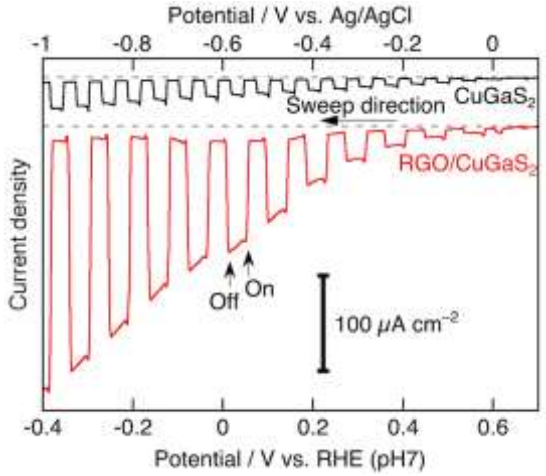

Figure 2 *I-V* curves of $CuGaS_2$ and RGO-$CuGaS_2$ composite photoelectrodes under visible light irradiation. Electrolyte: 0.1 mol L^{-1} K_2SO_4 aq., light source: 300 W Xe lamp with a long-pass filter (λ>420 nm).

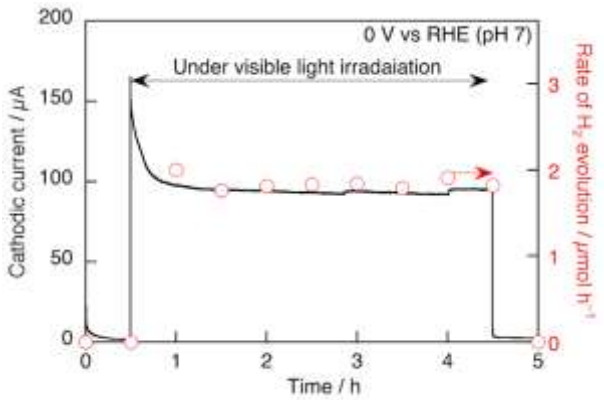

Figure 3 Cathodic current (left axis) and the rate of hygrogen evolution (right axis) using a RGO-$CuGaS_2$ composite photoelectrode (area 1.8 cm^2) under visible light irradiation. Electrolyte: 0.1 mol L^{-1} K_2SO_4 aq., light source: 300 W Xe lamp with a long-pass filter (λ>420 nm).

photocatalysts were used.[9,10] Figure 1C shows SEM image of the collected powder after visible light irradiation. The RGO sheets and $CuGaS_2$ particles were attached to each other. These characterizations revealed that RGO-$CuGaS_2$ composite was successfully obtained. Additionally, no change in the absorption edge of $CuGaS_2$ between with and without RGO was observed (Figure S2), indicating that the RGO did not affect the energy structure of $CuGaS_2$.

2. Photoelectrochemical performance of RGO-$CuGaS_2$ composite under visible light irradiation

The obtained composite was pasted on a FTO conductive substrate by a drop-casting method and subsequent calcination in a N_2 atmosphere. Figure 2 shows the photoelectrochemical performance of the RGO-$CuGaS_2$ composite. Pristine $CuGaS_2$ electrode showed cathodic photocurrent under visible light irradiation. The cathodic photocurrent was dramatically improved by incorporating RGO. As a reference, the photoelectrochemical performance of a physical mixture of a commercial conductive carbon black and $CuGaS_2$ was also

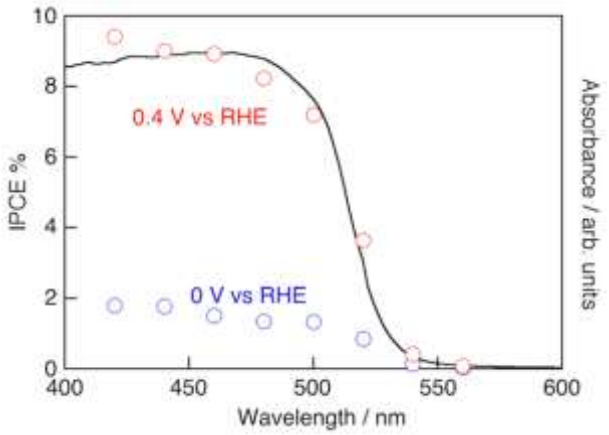

Figure 4 Action spectra of RGO-$CuGaS_2$ composite photoelectrode and a diffuse reflectance spectrum of $CuGaS_2$. Electrolyte: 0.1 mol L^{-1} K_2SO_4 aq., light source: 300 W Xe lamp with band-pass filters.

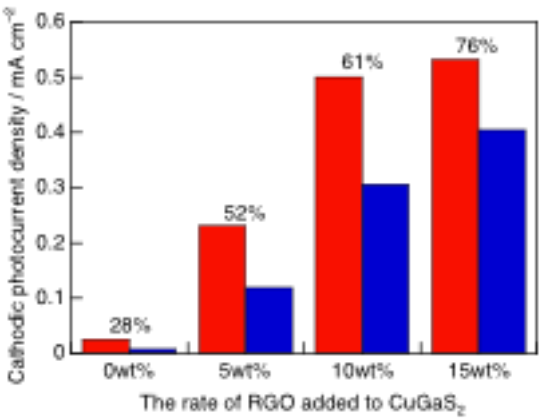

Figure 5 Cathodic photocurrent of RGO-$CuGaS_2$ composite photoelectrode with various loading rates of RGO under visible light irradiation from an FTO substrate side (left bar) and a particle side (right bar). The percentages on the bars represent the rate of the photocurrent obtained with irradiation from a particle side to that from an FTO substrate side. Potential: 0.9 V vs. RHE (pH7), electrolyte: 0.1 mol L^{-1} K_2SO_4 aq., light source: 300 W Xe lamp with a long-pass filter (λ>420 nm).

evaluated. However, no enhanced photocurrent was observed. This indicates the advantage of RGO with the characteristic large two-dimensional sheet to obtain well contact with many $CuGaS_2$ particles.

In order to exclude the possibility that the increased cathodic photocurrent is due to the further reduction of RGO, the evolved gas was analyzed using GC. H_2 evolved under visible light irradiation corresponding with the cathodic photocurrent as shown in Figure 3. This almost 100% of Faradaic efficiency indicates that the cathodic photocurrent is due to the water reduction to produce H_2. Moreover, we have analyzed the metal cation species in the electrolyte by ICP after 6h of photoelectrochemical measurement under similar condition of Figure 3 to clarify the stability of RGO-$CuGaS_2$ photoelectrode. No detection of Cu and Ga ions indicated that those ions did not leach from $CuGaS_2$ particles.

The onsets of IPCEs of the RGO-$CuGaS_2$ composite electrode measured at both 0 V and 0.4 V vs. RHE (pH 7) agreed well with the absorption edge of $CuGaS_2$ as shown in

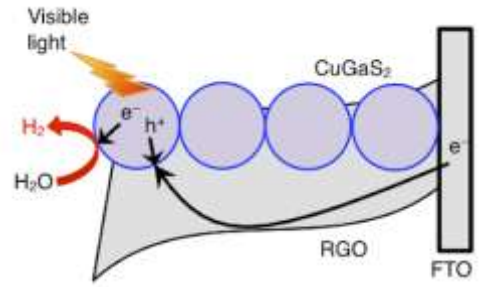

Figure 6 Expected electron flow in a RGO-$CuGaS_2$ composite electrode under photoirradiation.

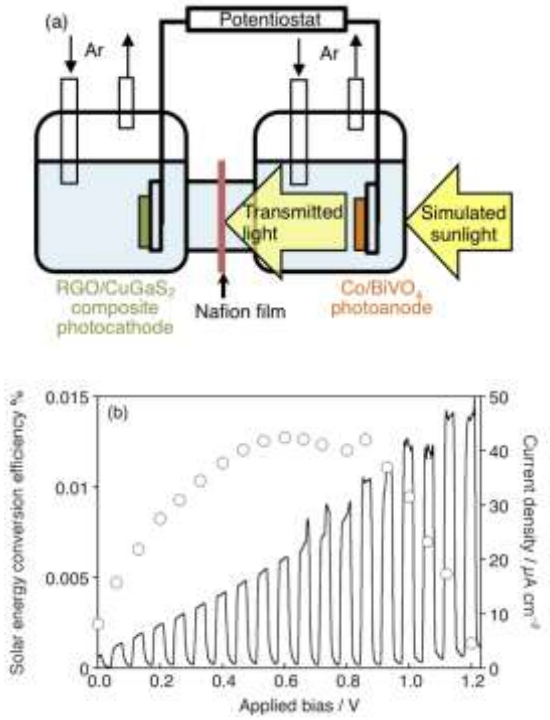

Figure 7 (a) H-type glass cell for the electrochemical water splitting using RGO-$CuGaS_2$ photocathode (1.9 cm^2) and CoOx-loaded $BiVO_4$ photoanode (1.1 cm^2). The photocathode and the photoanode were set parallel to each other. The photoelectrodes were irradiated from the photoanode side. (b) Solar energy conversion efficiency (left axis) and current measured using a photoelectrochemical cell consisting of RGO-$CuGaS_2$ composite photocathode and CoOx-loaded $BiVO_4$ photoanode. Electrolyte: aqueous buffer solution containing dissolved KH_2PO_4 and Na_2HPO_4 (pH7), light source: simulated sunlight (AM 1.5, 100 mW).

Figure 4. This agreement indicates that the cathodic photocurrent was generated accompanied with the band gap photoexcitation of $CuGaS_2$. This result indicates that the RGO-sensitized reaction proposed in an RGO-TiO_2 system[20,22] did not proceed at least in our composite electrode system.

Figure 5 shows the effect of the amount of the RGO on the photocurrent of the composite photoelectrode irradiated with visible light from an FTO transparent substrate side and a particle side of the photoelectrode. The percentages on the bars represent the rate of the photocurrent obtained with irradiation from a particle side to that from an FTO substrate side. Again, all of the RGO-$CuGaS_2$ composite photoelectrodes showed higher cathodic photocurrent than the pristine $CuGaS_2$ photoelectrode. The photocurrent was improved with an increase in the amount of the RGO. Additionally, the rate of the photocurrent obtained with irradiation from a particle side to that from an FTO substrate side also increased with the increase in the amount of RGO. This clearly indicates the role of RGO in the RGO-$CuGaS_2$ composite photoelectrode as discussed in detail below. Laser scanning microscope observation revealed that the thickness of the RGO-$CuGaS_2$ composite photoelectrode was about 2–3 μm. Additionally, the absorption coefficient of the $CuGaS_2$ at the visible range is 20,000–50,000 cm^{-1}.[23] The thickness of the photoelectrode and the absorption coefficient suggest that the particles far from the FTO substrate were mainly excited, when the photoelectrode was irradiated with visible light from a particle side. Therefore, in the $CuGaS_2$ photoelectrode without RGO, most of photogenerated holes could not reach the FTO substrate because of a long way to FTO substrate with high resistance. In contrast, in the RGO-$CuGaS_2$ composite photoelectrode, photogenerated holes in the particles far from the FTO substrate were efficiently consumed by electrons delivered from the FTO substrate to particles through the RGO as shown in Figure 6. Therefore, the rate of the photocurrent obtained with irradiation from a particle side to that from a FTO substrate side also increased as the amount of RGO increased. The remained photoexcited electrons reduced water to H_2 on the particle surface. The reduction of internal resistance of a $CuGaS_2$ photoelectrode by incorporation of RGO was supported by the electrochemical impedance spectroscopy (Figure S3), as observed in RGO-TiO_2 photoelectrode.[24] Thus, the RGO enhanced the electrochemical performance for the reduction of water to H_2 over the $CuGaS_2$ photoelectrode. In the RGO-photoanode systems such as RGO-TiO_2, RGO-$BiVO_4$, and RGO-WO_3, the RGO promotes the electron migration from photocatalyst particles to a conductive substrate.[9–12] The present study revealed that the incorporation of RGO is also an effective strategy to enhance a photocathodic process.

3. Photoelectrochemical cell combined RGO-$CuGaS_2$ composite photocathode with CoOx-loaded $BiVO_4$ photoanode

The RGO-$CuGaS_2$ composite photocathode possessed electrochemically-sufficient onset potential to fabricate a photoelectrochemical cell using a CoOx-loaded $BiVO_4$ photoanode for water splitting without an external bias (Figure S4). Figure 7 shows the *I-V* curve of the photoelectrochemical cell using RGO-$CuGaS_2$ composite of a photocathode and CoOx-loaded $BiVO_4$ of a photoanode under simulated sunlight irradiation. The photoelectrochemical cell gave photocurrent. The photocurrent increased with applying larger bias between the photocathode and the photoanode. Most interestingly, the photocurrent was obvious even without any external bias. Gas phase analysis revealed that the certain H_2 evolved is corresponding to the observed photocurrent (Figure S5). Unfortunately, O_2 was not detected probably due to the low photocurrent and the low sensitivity of our GC with an Ar carrier which is similar thermoconductivity to O_2. However, the $BiVO_4$ photoelectrode is widely known as a promising

photoanode for water oxidation to form O_2.[17,25–27] Therefore, the experimental situation and condition suggest that solar water splitting using the photoelectrochemical cell without any external bias was achieved.

Conclusions

RGO-$CuGaS_2$ composite was successfully obtained by photocatalytically reducing graphene oxide to reduced graphene oxide (RGO) over $CuGaS_2$ particles under visible light irradiation. The RGO-$CuGaS_2$ composite photoelectrode showed higher cathodic photocurrent under visible light irradiation than a pristine $CuGaS_2$ photoelectrode. The rate of H_2 evolution agreed well with the theoretical rate calculated from the observed cathodic photocurrent, indicating that RGO was not further reduced during the photoelectrochemical reaction and the photocurrent was used for water reduction. The wavelength dependency revealed that the photocurrent was generated accompanied with band gap photoexcitation of $CuGaS_2$. The photoelectrochemical cell consisting of the enhanced RGO-$CuGaS_2$ composite photocathode and a CoOx-loaded $BiVO_4$ photoanode gave photocurrent under simulated sunlight irradiation without any external applied bias. Thus, the present study demonstrated the potential of the reduced graphene oxide for enhancing a photoelectrochemical performance of a powder-based metal sulfide photocathode for solar water splitting. This present study provides a new way of utilizing metal sulfide materials for photoelectrochemical solar water splitting by incorporating the reduced graphene oxide.

Acknowledgements

This work was supported by Grant-in-Aid (no. 24107004) for Scientific Research on Innovative Areas (no. 2406) and Grant-in-Aid for Young Scientists (B) (no. 26820354) from the Ministry of education, Culture, Sports, Science & Technology in Japan and ENEOS Hydrogen Trust Fund.

Notes and references

[a] Department of Applied Chemistry, Faculty of Science, Tokyo University of Science, 1-3 Kagurazaka, Shinjuku-ku, Tokyo 162-8601, Japan

[b] Photocatalysis international Research Center, Research Institute for Science and Technology, Tokyo University of Science, 2641 Yamazaki, Noda-shi, Chiba 278-8510, Japan

[c] ARC Centre of Excellence for Functional Nanomaterials, School of Chemical Engineering, The University of New South Wales, Sydney, NSW 2052, Australia

† Electronic Supplementary Information (ESI) available: [XRD patterns, additional photoelectrochemical experiments. See DOI: 10.1039/b000000x/

1 H.E. Osterloh, *Chem. Mater.*, 2008, **20**, 35.
2 A. Kudo, Y. Miseki, *Chem. Soc. Rev.*, 2009, **38**, 253.
3 Y. Inoue, *Energy Environ. Sci.*, 2009, **2**, 364.
4 R. Abe, *Photochem. Photobiol. C*, 2010, **11**, 179.
5 K. Zhang, L. Guo, *Catal. Sci. Technol.*, 2013, **3**, 1672.
6 S. Ikeda, T. Nakamura, S.M. Lee, T. Yagi, T. Harada, T. Minegishi, M. Matsumura, *ChemSusChem*, 2011, **4**, 262.
7 Gunawan, W. Septina, S. Ikeda, T. Harada, T. Minegishi, K. Domen, M. Matsumura, *Chem. Commun.*, 2014, **50**, 8941.
8 A. Iwase, A. Kudo, *J. Mater. Chem.*, 2010, **20**, 7536.
9 Y.H. Ng, A. Iwase, A. Kudo, R. Amal, *J. Phys. Chem. Lett.*, 2010, **1**, 2607.
10 Y.H. Ng, I.V. Lightcap, K. Goodwin, M. Matsumura, P.V. Kamat, *J. Phys. Chem. Lett.*, 2010, **1**, 2222.
11 N.J. Bell, Y.H. Ng, A. Du, H. Coster, S.C. Smith, R. Amal, *J. Phys. Chem. C*, 2011, **115**, 6004.
12 Y.H. Ng, A. Iwase, N.J. Bell, A. Kudo, R. Amal, *Catal. Today*, 2011, **164**, 353.
13 B. Tell, J.L. Shay, H.M. Kasper, *Phys. Rev. B*, 1971, **4**, 2463.
14 B. Tell, J.L. Shay, H.M. Kasper, *J. Appl. Phys.*, 1972, **43**, 2469.
15 A. Marti, D.F. Marron, A. Luque, *J. Appl. Phys.*, 2008, **103**, 073706.
16 W.S. Hummers, R.E. Offeman, *J. Am. Chem. Soc.*, 1958, **80**, 1339.
17 Q. Jia, K. Iwashina, A. Kudo, *Proc. Natl. Acad. Sci.*, 2012, **109**, 11564.
18 S. Stankovich, D.A. Dikin, R.D. Piner, K.A. Kohlhaas, A. Kleinhammes, Y. Jia, Y. Wu, S.T. Nguyen, R.S. Ruoff, *Carbon*, 2007, **45**, 1558.
19 G. Williams, B. Seger, P.V. Kamat, *ACS Nano*, 2008, **2**, 1487.
20 K.K. Manga, Y. Zhou, Y. Yan, K.P. Loh, *Adv. Funct. Mater.*, 2009, **19**, 3638.
21 Y. Matsumoto, M. Koinuma, S.Y. Kim, Y. Watanabe, T. Tanicguchi, K. Hatakeyama, H. Tateishi, S. Ida, *ACS Appl. Mater. Interfaces*, 2010, **2**, 3461.
22 R. Long, N.J. English, O.V. Prezhdo, *J. Am. Chem. Soc*., 2012, **134**, 14238.
23 S. Levcenko, N.N. Syrbu, V.E. Tezlevan, E. Arushanov, S. Doka-Yamigno, Th. Schedel-Niedrig, M.Ch. Lux-Steiner, *J. Phys.: Condens. Matter*, 2007, **19**, 456222.
24 C. Zhai, M. Zhu, Y. Lu, F. Ren, C. Wang, Y. Du, P. Yang, *Phys. Chem. Chem. Phys*. 2014, **16**, 14800.
25 F.F. Abdi, L. Han, A.H.M. Smets, M. Zeman, B. Dam, R. van de Krol, *Nature Commun*. 2013, **4**, 2195.
26 T.W. Kim, K.S. Choi, *Science* 2014, **343**, 990.
27 Y. Pihosh, I. Turkevych, K. Mawatari, T. Asai, T. Hisatomi, J. Uemura, M. Tosa, K. Shimamura, J. Kubota, K. Domen, T. Kitamori, *Small* 2014, **10**, 3692.